GSA Data Repository 2015074

Shaking water out of soils

SUPPLEMENTARY INFORMATION

Christian H. Mohr[1,2], Michael Manga[2], Chi-yuen Wang[2], James W. Kirchner[2,3] and Axel Bronstert[1]

[1]*Institute of Earth- and Environmental Science, University of Potsdam, Potsdam 14476, Germany*

[2]*Department of Earth and Planetary Science, University of California, Berkeley, California 94720, USA*

[3]*Department of Environmental Sciences, Swiss Federal Institute of Technology, ETH, Zürich 8092, Switzerland*

Corresponding author

Christian Mohr

Institute of Earth and Environmental Science

Geohazards Research Group

Karl-Liebknecht-Strasse 24-25

14476 Potsdam-Golm/ Germany

cmohr@uni-potsdam.de

Tel.: +49-331-977-2254

Fax.: +49-331-977-2068

METHODS

Observation of streamflow, rainfall and soil moisture.

Streamflow discharge was monitored by a flume equipped with a custom-built water stage recorder with a resolution of 2 mm. The sampling interval was 10 minutes. Rainfall was recorded by a Hobo tipping bucket rain gauge close to the streamflow gauging station and at a meteorological station about 600 m north of the catchment. The rain gauge registers data with an accuracy of 0.2 mm. Soil moisture was manually estimated using a mobile TDR-Trime-Probe (IMKO) along transects of access tubes in 10 cm depth increments up to a maximum depth of 270 cm below surface. Access tubes were installed only in various adjacent catchments. There, the number of access tubes ranged between 6 and 15. The last soil moisture measurements before the earthquake were carried out on February 19th 2010.

Rescaling of evapotranspiration rates and normalization of discharge

Evapotranspiration rates were rescaled using potential evapotranspiration ET_{pot} estimated by Penman-Monteith and a scale factor s:

$$ET_{rescaled}(mm/h) = ET_{pot} * s \quad \text{with} \quad s = \frac{[average(P) - average(Q)]}{average[ET_{pot}]} \qquad \text{(eq. 1 and 2)}$$

Amplitudes of daily cycling of streamflow discharge were normalized to daily average discharge according to:

$$Amplitude = \frac{[\max(Q) - \min(Q)]}{average[Q]} \qquad \text{(eq. 3)}$$

Modelling

Modelling of Groundwater flow

The equations for groundwater flow are solved numerically with an implicit finite difference method. Although they are geometrically simplified, 1-D models are commonly used to interpret hydrological responses to earthquakes (Wang, 2004; Manga, 2001; Wang, 2010).

Modelling of co-seismic water mobilization from the vadose zone

Co-seismic recharge *A(t)*, the excess water released per unit volume averaged across the catchment area, is modelled following Wang et al. (2004) by using a steep co-seismic arctangent saltus function

$$A = \left[\frac{\pi}{2} + \arctan c\,(t - t_0)\right] \qquad \text{(eq. 7)}$$

where the parameter c is fitted to the steepness of the increase of streamflow discharge and t_0 is the time of the earthquake.

In contrast to previous studies, we infer that the excess water mobilized by the earthquake comes at least partially from the vadose zone. Saturated flow is governed by Darcy's law (Hillel, 2003) and initiated when the negative pressure head (suction) that is expressed by matric potential Ψ_{matric} (adhesive intermolecular forces between water and soil solids and cohesive forces between the water molecules; Hillel, 2003) is exceeded by the seismic accelerations. Hence, an additional positive force is needed to release the capillary soil water from the pores. Seismic energy density e is defined as the maximum seismic energy available in a unit volume to do work on rock or sediment (Wang, 2010) and may be estimated by

$$\log_{10} e\left(J/m^3\right) = -3.03\log_{10} r + 1.45M - 4.24 \qquad \text{(eq. 8)}$$

with earthquake Magnitude *M* and the epicentral distance *r* in kilometres. The seismic energy density in equation (8) is expressed in J/m^3 and can be treated as a pressure head (Pa) counteracting the matric potential.

Given this key assumption and the parameter values of M=8.8 and r=115-130km, *e* yields 10^2-10^3 Pa acting as a positive pressure head ($\Psi_{seismic}$) and the static threshold of saturation θ dynamically evolves during shaking according to

$$\theta^{(\Psi_{seismic}+\Psi_{matric})} = \left[1+\left[\alpha*\left(\Psi_{seismic}+\Psi_{matric}\right)\right]^n\right]^{-1+\frac{1}{n}} \quad \text{(eq. 9)}$$

where α and n represent the Van Genuchten empirical texture-specific parameters (Van Genuchten, 1980).

As a result, flow conditions dynamically switch from an unsaturated to saturated state once the seismic energy density exceeds the matric potential ($\Psi_{seismic} \geq \Psi_{matric}$). In fact, this estimate is a lower bound since flow already initiates under unsaturated flow conditions by gravity and, thus, vertical drainage from the vadose zone is already expected when $\Psi_{matric} \leq \Psi_{seismic} + \Psi_{gravitational}$. Given the possibility to drain, the mobilized soil moisture recharges the aquifer during the shaking. Although the relation between the seismic energy density, earthquake magnitude and epicentral distance was derived for Southern California (Wang, 2007), we use it here as a first approximation, in the absence of a similar relation for Chile. The absence of a hydrological response to the Araucaria aftershock is consistent because its seismic energy density is much smaller – too small to release water from the vadose zone.

Inverse modelling of evapotranspiration

We estimated evapotranspiration by three different methods: (1) simple spline interpolation linking maximum daily discharge, (2) considering maximum recharge rates during night (White, 1932) and (3) by 'doing hydrology backwards' as proposed by Kirchner (2009).

Daily evapotranspiration was estimated as the difference between a spline interpolation linking daily maximum discharge rates – as expected without evapotranspiration losses during night – and the observed discharge rates including the evapotranspiration signal. In addition daily evapotranspiration rates were independently estimated by the method of White (1932) considering maximum recharge rates during night:

$$E_t = S_y\,(24r \pm sd) \qquad \text{(eq. 10)}$$

where S_y refers to a specific yield and r to the slope of the tangential line drawn to the increasing streamflow discharge (mm/h) during predawn/dawn times when E_t is negligible. Uncertainty is given by ± one standard deviation (*sd*). Assuming the streamflow increase is proportional to the rate of groundwater recharge to the riparian zone, we then extend the tangential line over a 24h period and take the difference to the streamflow discharge rates to estimate the total water recharge to the riparian buffer zone (Gribovszki, 2010). The estimated recharge rate must be modified by the difference in the observed streamflow discharge rates over the 24h-period because streamflow discharge only rarely reaches the rates of the previous day.

Finally, we calculated evapotranspiration rates E_t (t) following Kirchner's approach of "doing hydrology backwards", a modelling procedure based on observable fluxes assuming a catchment-specific relationship between discharge and storage rather than on point-scale measured soil-hydrologic properties (Kirchner, 2009). Here, evapotranspiration rates are a function of time and can be approximated using the conservation-of-mass equation when storage S (units of depth), precipitation P and discharge Q (both in units of depth per time) are known,

$$E_t = P - Q - \frac{\partial S}{\partial t} \qquad \text{(eq. 11)}$$

Assuming that discharge depends only on water storage across the catchment, the invertible relation between water storage and discharge can be written as

$$Q = f(S) \quad \leftrightarrow \quad S = f^{-1}(Q)$$

Hence, Q can be expressed by using a catchment-specific function of water storage, which relates changes in discharge Q to changes in catchment specific storage S

$$\frac{\partial Q}{\partial t} = \frac{\partial Q}{\partial S} * \frac{\partial S}{\partial t} = \frac{\partial Q}{\partial S}\left(P - E_t - Q\right) \qquad \text{(eq. 12)}$$

The term $\frac{\partial Q}{\partial S}$ is the derivative of the storage-discharge relationship $f(S)$ and expresses the sensitivity of discharge to changes in storage. Owing to the assumption that S is a function of Q, $\frac{\partial Q}{\partial S}$ can be considered as the discharge sensitivity function $g(Q)$

$$\frac{\partial Q}{\partial S} = f'(S) = f'\left(f^{-1}(Q)\right) = g(Q) \qquad \text{(eq. 13)}$$

The discharge sensitivity function can then be approximated from observed fluxes

$$g(Q) = \frac{\partial Q}{\partial S} = \frac{\partial Q / \partial t}{\partial S / \partial t} = \frac{\partial Q / \partial t}{P - E - Q} \qquad \text{(eq. 14)}$$

Once this catchment specific discharge sensitivity function $g(Q)$ is identified, changes in storage can be inferred and thus losses or gains from discharge Q, precipitation P or evapotranspiration E_t can be estimated from the discharge time series (Kirchner, 2009). In practice, $g(Q)$ is estimated as an empirical function from plotting the recession rate $\left(-\partial Q / \partial t\right)$ as a function of discharge Q. We approximated this function using a power law function of Q

$$g(Q) = \frac{\partial Q}{\partial S} = \frac{\partial Q / \partial t}{-Q} = a * Q^{b-1} \qquad \text{(eq. 15)}$$

with slope b and intercept a in which a reflects scaling, physical and/or geomorphic properties of the catchment (Rupp, 2006).

As no rainfall was recorded around the time of the earthquake ($P \approx 0$), evapotranspiration rates E_t are inferred by

$$E_t\big|_{P=0} = -\frac{\partial Q/\partial t}{g(Q)} - Q \approx -\frac{(Q_{t+1}-Q_{t-1})/2\,\partial t}{[g(Q_{t+1})+g(Q_{t-1})]/2} - (Q_{t+1}+Q_{t-1})/2 \quad \text{(eq. 16)}$$

for the time steps *t* (Kirchner, 2009).

In order to minimize the impact of evapotranspiration and rainfall fluxes on *g(Q)*, only discharge recession data during night within a period of no recorded rainfall 6h prior and at least 2hr after were considered to determine *g(Q)* (Kirchner, 2009). Owing to the lag effects of evapotranspiration on night-time streamflow during the dry season, the selection criteria were further expanded to rainless periods during the rainy season with relatively low evapotranspiration rates. In order to estimate the impact of *g(Q)* on evapotranspiration, a sensitivity analysis for *a* and *b* was conducted in the range of ± one standard error. The *g(Q)* function was also applied in a simplified way in order to increase sensitivity of E_t to $-\frac{\partial Q/\partial t}{g(Q)}$. Because *Q* is two orders of magnitude smaller than potential evapotranspiration and there was no rainfall, we assume *Q* and *P* are negligible which thus simplifies E_t to

$$E_t\big|_{P=0,\,Q<<Et} = -\frac{\partial Q/\partial t}{g(Q)} \approx -\frac{(Q_{t+1}-Q_{t-1})/2}{[g(Q_{t+1})+g(Q_{t-1})]/2} \quad \text{(eq.17)}$$

Possible earthquake effects on porosity were explored by comparing pre- and post-seismic discharge sensitivity functions *g(Q)*, since storage *S* is directly related to porosity (Freeze, 1979).

Daily evapotranspiration values for the periods from February 20th – 26th and February 28th – March 11th were compared and statistically tested by the Wilcoxon rank sum test at a significance level of alpha=5%. The relationship between changes in streamflow discharge amplitudes and changes in daily evapotranspiration before and after the earthquake was assessed by applying analysis of covariance at the same significance level.

159 **SUPPLEMENTARY FIGURES**

160

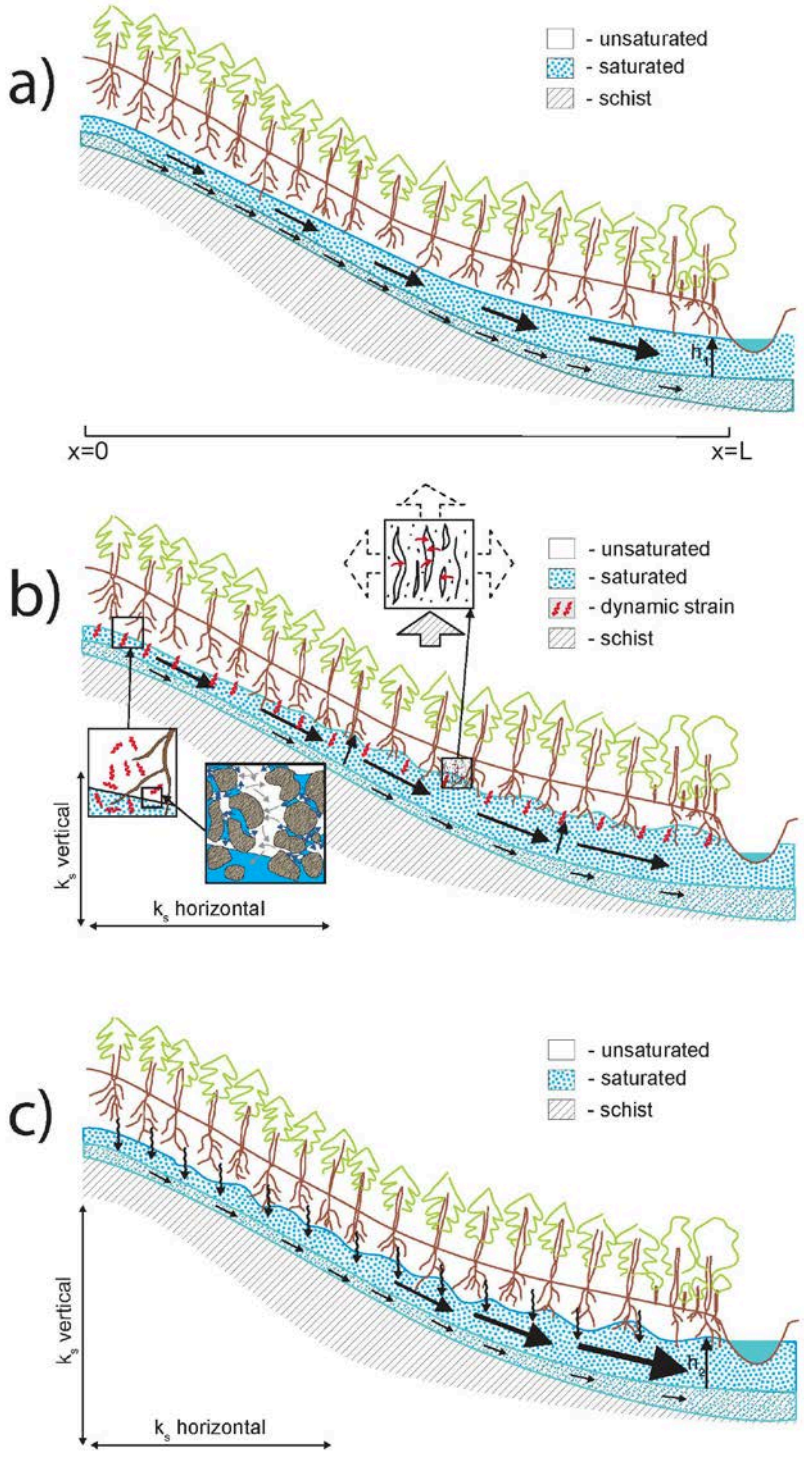

161

162

163 Supplement Figure 1. Conceptual model. (a) Prior the earthquake: Low baseflow conditions

164 (h_1 corresponds to the height of the cross-section of saturated zone) and plant-water

availability is limited to deep rooting riparian vegetation. Thus, plant activity is relatively low. Thickness of black arrows indicates relative volume of subsurface flow and dots indicate the saturation level of each geological unit. (b) During the earthquake: Ground shaking causes two effects. First, it dilates the shallowest sediments and forms cracks. Water then migrates from saturated pores into the new cracks (red arrows) lowering the hydraulic head until the dilatant cracks are filled. As a result, streamflow is temporarily disrupted. Further, dilatant cracking enhance vertical permeability and thus improves connectivity between vadose zone water and the groundwater flow zone. Second, ground shaking mobilizes vadose zone water when $\Psi_{matric} \leq \Psi_{seismic} + \Psi_{gravitational}$. (grey arrows in inset). Upon established connectivity between vadose zone and groundwater zone, the released water recharges the groundwater. Drainage is provided by preferential flow paths, e.g. root channels or soil cracks, clearing of clogged macro-pores by transient stresses from seismic waves and dilatant cracks. Horizontal permeability remains unchanged. (c) After the earthquake: As the released vadose zone water recharges the groundwater, the groundwater table rises (h_2) and extends the 'active zone' of high root-water-uptake along the valley bottoms. There, the available water resources promote plant activity along the riparian buffer strips as reflected in intensified diurnal streamflow oscillation. Further, the higher groundwater table increases streamflow discharge.

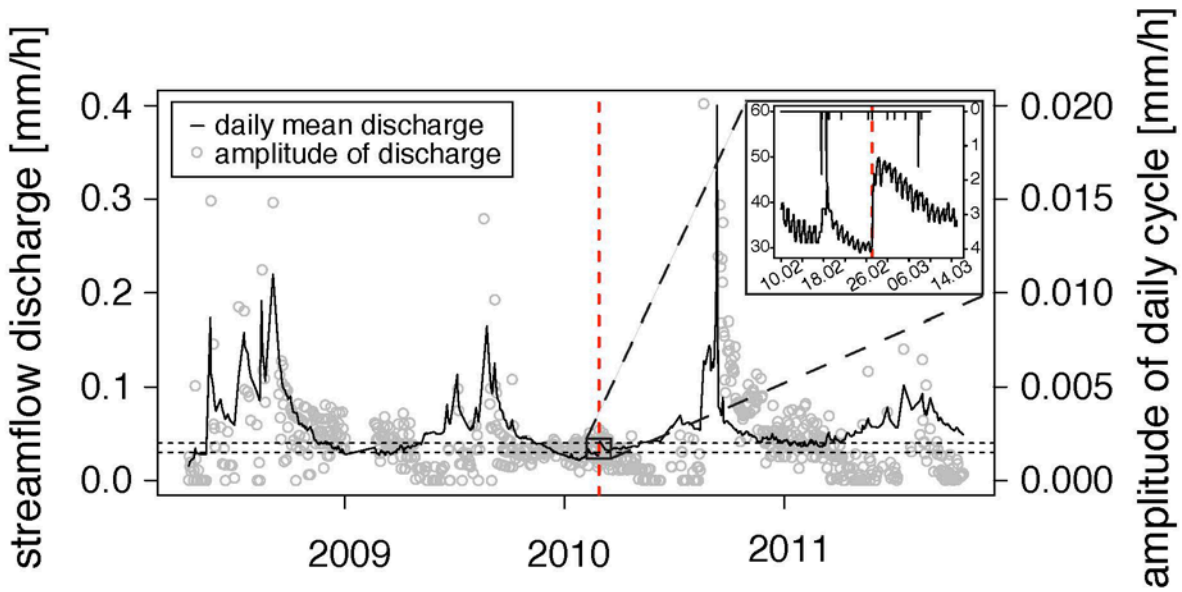

Supplement Figure 2. Daily mean streamflow discharge (mm/h) and amplitudes of diurnal streamflow cycling (mm/h) for the period from April 17th 2008 to October 25th 2011. The red dashed line shows the time of the earthquake. The black dashed horizontal lines indicate the range of streamflow discharge that was observed during the first days after the earthquake.

SUPPLEMENTARY TABLE

Supplementary Table 1. Estimated whole-catchment daily evapotranspiration (mm/day) by doing hydrology backwards, applying the approach by White and by spline interpolation.

Date	Hydrology backwards	White (1932)	Spline Interpolation
20.02.2010			0.033
21.02.2010	0.076	0.034	0.036
22.02.2010	0.073	0.033	0.030
23.02.2010	0.071	0.033	0.028
24.02.2010	0.069	0.033	0.030
25.02.2010	0.069	0.034	0.017
26.02.2010	0.069	0.033	0.030
27.02.2010	-	-	
28.02.2010	0.108	-	0.047
01.03.2010	0.109	0.048	0.028
02.03.2010	0.107	0.046	0.033
03.03.2010	0.104	0.047	0.042
04.03.2010	0.101	0.048	0.045
05.03.2010	0.099	0.049	0.042
06.03.2010	0.094	0.050	0.047
07.03.2010	0.094		0.033
08.03.2010	0.092		0.031
09.03.2010	0.088		0.043
10.03.2010	0.086		0.040